Ongoing Aeroelastic Prediction and Validation Activities at NASA Langley Research Center

Bret K. Stanford*, Kevin E. Jacobson†, and Pawel Chwalowski‡
NASA Langley Research Center, Hampton, VA, 23681

Current and future transonic aircraft concepts of interest to NASA may be susceptible to complex aeroelastic failure mechanisms that are difficult for computational tools to adequately predict. As such, a direct accounting of transonic flutter behavior has not historically been conducted at early design stages, where problems are less expensive to address. This paper summarizes efforts within NASA Langley's Aeroelasticity Branch to improve this situation, through advancements in computational prediction and optimization of transonic flutter behavior, in addition to planned wind tunnel tests aimed at providing a greater wealth of experimental data to validate predictions.

I. Introduction

There is a need to push higher-fidelity aeroelastic physics earlier into the design process for fixed wing aircraft. Specifically, a proper accounting of transonic aeroelastic flutter at earlier design stages can help ensure against costly flutter problems encountered late in the aircraft design process,[1] and also help alleviate the costs of late-stage wind tunnel and flight flutter test campaigns.[2] Furthermore, nontraditional vehicle concepts under consideration for future development may be more flutter-critical than current aircraft (e.g., large wing spans for drag-reduction purposes); for these vehicles, it may not be possible to properly design the vehicle using flutter predictions from lower-fidelity aeroelastic analysis tools. In the authors' view, there are three barriers to the use of transonic aeroelastic flutter predictions at early design stages: (1) an inability to efficiently compute transonic flutter boundaries for realistic configurations; (2) an inability to efficiently conduct large-scale computational design with flutter constraints; (3) a lack of experimental data with which to validate predictions.

The current state-of-the-practice in Computational Fluid Dynamics (CFD)-based flutter predictions involves repeated time integration of the unsteady Reynolds-averaged Navier-Stokes (uRANS) equations, at progressively higher dynamic pressures, until an oscillatory instability is observed. This process is expensive and cumbersome, particularly when wrapped within a gradient-based design optimization process. Furthermore, the extent to which uRANS-based predictions and designs can handle flutter behavior driven by shock/boundary-layer interactions[3] is not always clear, but experimental test cases commonly used for validation/benchmarking suffer from various flaws. These issues include: test cases with overly-weak flow nonlinearities;[4,5] overly-simple geometries and structures;[6] a lack of actual published data (i.e., data needed to verify all aspects of the experiment, rather than just the final flutter boundary);[7,8] a lack of detail/availability of the problem definition.[9]

The goals of this paper are to provide an overview of current and planned activities at NASA Langley's Aeroelasticity Branch aimed at addressing each of the three barriers listed above. For more efficient flutter predictions, new computational tools have been developed[10] that allow for uRANS-based computations via a linearized frequency-domain (LFD) method. LFD methods have the potential to substantially decrease computational cost relative to time-marching schemes, provide a more "direct" flutter solution (i.e., concise flutter boundary prediction from a code, rather than via bracketing and interpolation), and can provide deeper insight into the aeroelastic mechanisms. Efficient adjoint methods have also been developed for LFD tools,[11] to enable large-scale gradient-based design optimization with flutter constraints.

*Research Aerospace Engineer, Aeroelasticity Branch, bret.k.stanford@nasa.gov, AIAA Associate Fellow.
†Research Aerospace Engineer, Aeroelasticity Branch, AIAA Member.
‡Research Aerospace Engineer, Aeroelasticity Branch, AIAA Senior Member.

To address shortcomings in the current state of aeroelastic validation, NASA Langley has organized the Aeroelastic Prediction Workshop (AePW), currently in its 3rd iteration[a]. AePW provides a means to engage the international aeroelasticity community to define and to analyze challenge problems and to present results in a workshop setting. The results of the workshop, building on the two previous iterations,[12,13] help identify needs and improve the state-of-the-art in computational aeroelasticity, and develop better synergies between future wind tunnel experiments and computations. Of the various working groups involved in AePW3, NASA Langley leads the High Angle of Attack Working Group, specifically aimed at transonic flutter problems.

NASA Langley is also planning a series of wind tunnel tests for the Transonic Dynamics Tunnel (TDT). These tests are being planned as validation experiments,[14] and also to assess the use of optical methods in the TDT. Planned TDT entries include a test of the Coe generic launch vehicle,[15] a retest of the benchmark supercritical wing (BSCW),[6] and the design, fabrication, and test of an aeroelastic Common Research Model.[16] These tests present a building block approach of progressively-complex models (rigid model, rigid model attached to a pitch-plunge apparatus, flexible model) to incrementally validate targeted aspects of the computational aeroelastic predictions. One modeling aspect in particular that can be addressed with these test results, is the utility of conducting aeroelastic predictions within numerical models of the TDT itself, as opposed to modeling the aeroelastic articles in "free-air." The latter option is substantially less complex and expensive, but may not be able to adequately predict the aeroelastic physics measured in the TDT, for some configurations.

II. Aeroelastic Analysis

The current state-of-the-practice for CFD-based flutter predictions[17] utilizes the uRANS equations coupled to a modal representation of the structure. First, the steady flow equations are converged over the rigid wing surface. Second, a static aeroelastic computation is obtained, either by loosely coupling a steady flow solution to a steady structural (modal) solution, or by time-integrating the coupled equations with modal dampings set to large values. Finally, a dynamic aeroelastic solution is obtained by perturbing the modal parameters about the converged static aeroelastic solution. If the generalized modal displacements display an oscillatory decay in time, the entire process can be repeated, from the beginning, at a higher dynamic pressure q, which acts as a gain factor between the aerodynamic and structural disciplines. The process is repeated until an oscillatory growth is observed, and then flutter-q is finally computed by bracketing the final two simulations, using damping values estimated from the output.[18] An example of this process can be seen in Fig. 1, where the aeroelastic response through 1 s corresponds to the static aeroelastic response (large prescribed modal damping values), followed by a perturbed dynamic response.

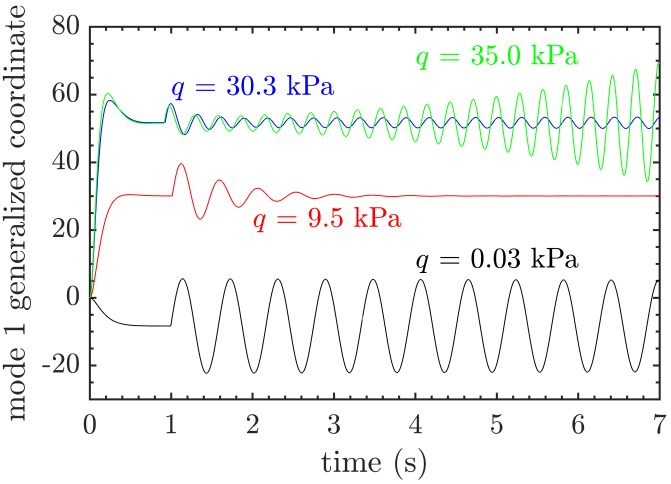

Figure 1: Sample dynamic aeroelastic time integration process, taken from Ref. 19.

Beyond the overall high cost of unsteady CFD computations, this workflow is not ideal for the following reasons. First, the flutter-q is not computed directly, as the outcome of a computational process, but is

[a] https://nescacademy.nasa.gov/workshops/AePW3/public/

instead bracketed from time-domain simulations. As tighter bracketing is desired (i.e., greater precision in flutter-q), more simulations must be conducted near the zero-damping flutter point, and these simulations must be run out for longer time periods, given the light damping. Second, the damping values estimated from the modal output can be sensitive to the modal perturbation and the window of time used for estimation. Third, the process does not necessarily give insight into competing flutter mechanisms, as the modal damping observed will be dominated by the critical flutter mechanism. Fourth, the process is subject to the typical time step convergence requirements, necessitating small time steps to resolve the CFD time scales, but long time records to observe the response of lightly damped, low frequency modes.

An alternative to time-domain simulations is the linearized frequency-domain (LFD) method: upon computing a converged static aeroelastic solution, infinitesimal oscillatory modal perturbations are conducted at a range of preselected frequencies. The uRANS equations are written as:

$$\boldsymbol{A}(\boldsymbol{q}, \dot{\boldsymbol{q}}, \boldsymbol{x}_G, \dot{\boldsymbol{x}}_G) := \boldsymbol{M}(\boldsymbol{q}, \boldsymbol{x}_G, \dot{\boldsymbol{x}}_G) \cdot \dot{\boldsymbol{q}} + \boldsymbol{R}(\boldsymbol{q}, \boldsymbol{x}_G, \dot{\boldsymbol{x}}_G) = \boldsymbol{0}, \tag{1}$$

where $\boldsymbol{q}$ is the flow state vector, $\boldsymbol{x}_G$ is the vector of volume mesh coordinates, $\boldsymbol{R}$ is the spatial residual, $\boldsymbol{M}$ is the mass matrix, and $\boldsymbol{A}$ is the complete unsteady flow residual. One can then assume small oscillatory perturbations of the form $\boldsymbol{x}_G = \boldsymbol{x}_{G_0} + \sum_{j=1}^{n} \hat{\boldsymbol{x}}_{G_j} \cdot e^{i \cdot \omega \cdot t}$, and $\boldsymbol{q} = \boldsymbol{q}_0 + \sum_{j=1}^{n} \hat{\boldsymbol{q}}_j \cdot e^{i \cdot \omega \cdot t}$, where (for example) $\boldsymbol{q}_0$ is a steady-state solution, $\hat{\boldsymbol{q}}$ is a Fourier coefficient, and ω is the oscillation frequency. Each Fourier coefficient corresponds to a structural mode shape of interest. Using these assumptions, the LFD equations can be written as:

$$\boldsymbol{A}_{LFD,j}\left(\boldsymbol{x}_{G_0}, \boldsymbol{q}_0, \hat{\boldsymbol{x}}_{G_j}, \hat{\boldsymbol{q}}_j, \omega\right) := \left(i \cdot \omega \cdot \boldsymbol{M}|_{\boldsymbol{x}_{G_0}, \boldsymbol{q}_0} + \left.\frac{\partial \boldsymbol{R}}{\partial \boldsymbol{q}}\right|_{\boldsymbol{x}_{G_0}, \boldsymbol{q}_0}\right) \cdot \hat{\boldsymbol{q}}_j + \left(i \cdot \omega \cdot \left.\frac{\partial \boldsymbol{R}}{\partial \dot{\boldsymbol{x}}_G}\right|_{\boldsymbol{x}_{G_0}, \boldsymbol{q}_0} + \left.\frac{\partial \boldsymbol{R}}{\partial \boldsymbol{x}_G}\right|_{\boldsymbol{x}_{G_0}, \boldsymbol{q}_0}\right) \cdot \hat{\boldsymbol{x}}_{G_j} = \boldsymbol{0}. \tag{2}$$

Equation 2 represents a linear complex-valued system of equations, which must be solved once for each structural mode shape j and each frequency value ω of interest. The complex-valued oscillatory flow fields $\hat{\boldsymbol{q}}_j$ can be used to compute a set of generalized aerodynamic forces (GAFs). These GAFs are identical in form to those output from a "classical" linear aeroelastic analysis built on the inviscid doublet lattice method (DLM), and may be used to directly solve for the flutter-q via a $p-k$ eigen-analysis. Previous work conducted on the LFD form of the uRANS equations can be found in Refs. 20 and 21, and has recently been implemented[10] around a stabilized finite element (SFE) solver[22] embedded within the FUN3D software.[23] In addition to providing deeper and more illustrative insight into the behavior of multiple potential flutter mechanisms (via solution of the $p-k$ equations), the LFD method is less expensive relative to time-domain simulations; the precise cost benefit depends on many factors, including the number of frequencies and number of mode shapes of interest.

Unsteady GAFs of the AGARD 445.6 case[4] are shown in Fig. 2 for comparison between LFD and the linear DLM method, where a good agreement between the two solvers is expected on account of the thin wing at a subsonic condition (i.e., minimal flow nonlinearity). Having computed the GAFs, the $p-k$ method can be used to compute the eigenvalue migration as a function of q; an example of this is shown for the Benchmark Supercritical Wing (BSCW)[13] in Fig. 3, where the flutter-q is identified when a root migrates from negative real part (stable) to positive (unstable). This process can be repeated at multiple Mach numbers to map out the entire flutter boundary, as shown in Fig. 4 for the Benchmark 0012 Wing.[24] For situations where 1) the transonic nonlinearities are strong and 2) there is an appreciable static aeroelastic disturbance (i.e., a lifting flow), it may be necessary to iterate between the static aeroelastic solution and the flutter solution, to ensure that the q value at which the static aeroelastic solution is run, is identical to the flutter-q. For situations where the the two criteria above are not met, it may be acceptable for the two q values to be mismatched.

Work has also been conducted towards integrating LFD-obtained flutter solutions into a mesh adaptation process, as summarized in Ref. 25. Multiscale mesh adaptation evolves the mesh based on a tensor metric that represents interpolation error of a scalar field such as Mach number or pressure. LFD-based flutter analyses are well-suited for mesh adaptation, given the fact that the multiscale metric can be computed from the fluttering flow field reconstructed from the $p-k$ eigenvectors. An example of this is shown in Figures 5 and 6 for the aeroelastic undeflected Common Research Model (uCRM),[16] where the latter figure shows the complex-valued flutter mode shape and surface pressures. The shock structures, and oscillatory

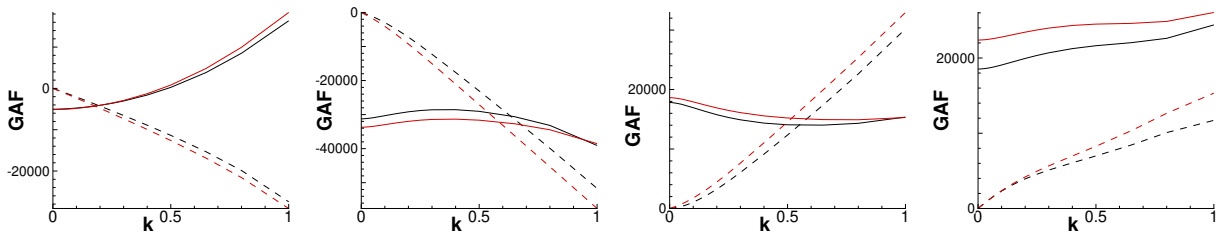

(a) A11 (b) A12 (c) A13 (d) A14

Figure 2: Generalized aerodynamic forces for the AGARD 445.6 wing at Mach=0.6: FUN3D/SFE LFD GAFs (black) and DLM GAFs (red), with solid and dashed lines as the real and imaginary parts, respectively.

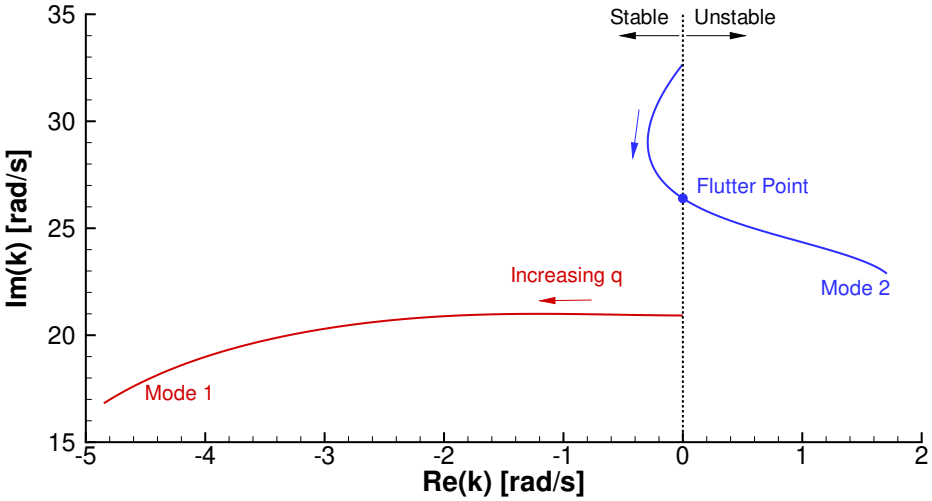

Figure 3: Root-locus plot for the Benchmark Supercritical Wing at Mach=0.74, AoA=0.0°.

perturbations to those shock structures, are extremely well resolved by the mesh adaptation process over the uCRM surface.

In addition to the test cases listed above, the LFD tool has successfully been used for additional vehicle configurations of interest to NASA, including the Integrated Adaptive Wing Technology Maturation project,[26] and the X-56A,[27] in both cases providing deeper insight into the fluttering behavior (through eigenvalue migration diagrams such as seen in Fig. 3) at a reduced cost relative to time-domain analysis. However, there are limits to the validity of the LFD tool: namely that the RANS-based steady flow and the subsequent linearized dynamics are reasonable representations of the system. For flows where the unsteadiness is inherently nonlinear or the steady RANS equations are not accurately modeling the flow, a time-domain approach must again be considered. It is further likely for these separated flows that uRANS-based solvers in general will be invalid. More work is needed to better understand the validity range of uRANS/LFD solvers for predicting flutter under separated flows, and at what point more costly tools like eddy-resolving CFD are required.

To address the shortcomings of uRANS methods, recent work has considered higher fidelity delayed detached eddy simulations (DDES)[28] for aeroelastic flutter computations, focused on the BSCW as shown in Fig. 7. One of the enabling technologies to making eddy-resolving CFD like DDES more tractable for aeroelastic simulation is a GPU port of the FUN3D finite-volume flow solver.[30] A form of the FUN3D mesh deformation based on superposition of the volume mesh motion due to each structural mode has been ported to the GPU to enable aeroelastic computations utilizing the GPU.[31] The GPU version of a hypersonic vehicle flutter analysis provided a normalized speedup of 39.3x for a GPU node with 6 NVIDIA V100 GPUs when compared to a dual-socket Intel Xeon 8168 node or a normalized speed up of 6.6x.[31] These types of improvements are indispensable because of the much finer meshes and timesteps required to properly apply eddy-resolving CFD methods.

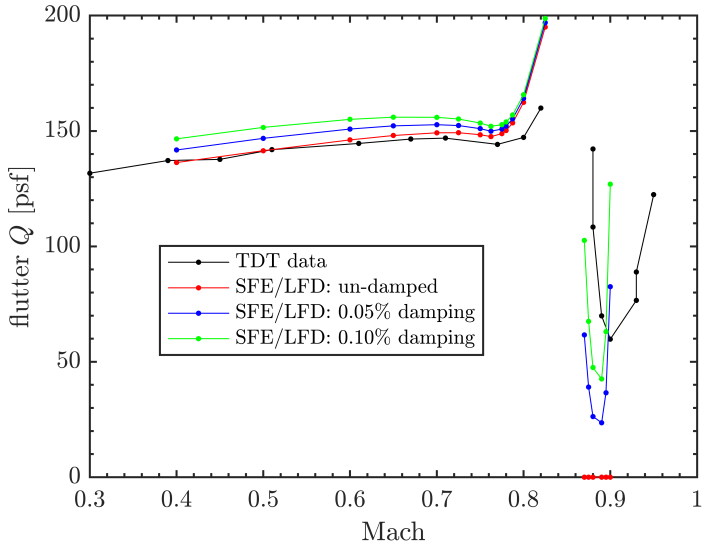

Figure 4: Flutter-q boundaries for different structural damping values of the Benchmark 0012 Wing, AoA=0.0°.

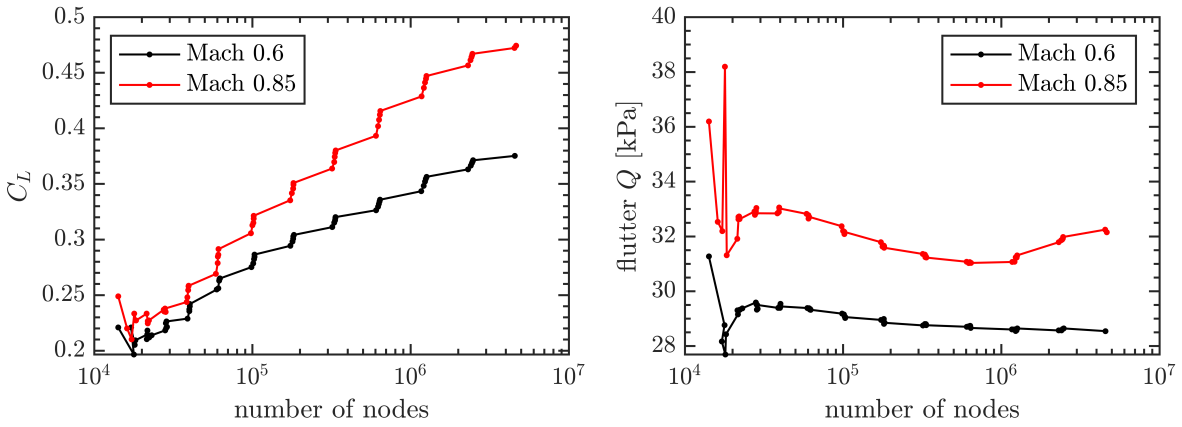

Figure 5: Steady lift coefficient (left) and flutter-q convergence across the mesh adaptation process, for the uCRM.

III. Aeroelastic Design

Having derived cost-efficient methods for computing aeroelastic flutter mechanisms, it is then of interest to use those tools for design. For costly high-fidelity simulations, gradient-based optimization is often the only tractable choice, where those gradients (i.e., the derivative of flutter-q with respect to design parameters) must be computed analytically, in such a way that the computational cost scales weakly with the number of design parameters (i.e., adjoint schemes). For time-domain aeroelasticity, adjoint derivatives have been demonstrated in Refs. 29-33, but the computational cost of these schemes is high, as the adjoint equations must be integrated in reverse-time. At each time step, the adjoint equations depend upon the primal solution (i.e., $\boldsymbol{q}$, etc), and so this primal solution must be stored to disk; in situations where such a storage scheme is intractable, checkpointing[34] may be used.

The scheme needed to compute the adjoint derivative of the LFD output (flutter-q) is overall less expensive relative to time-domain methods, but complications arise from the complex-valued nature of the equations, and also the fact that derivatives are sought for a system that has already been linearized (Eq. 2), and

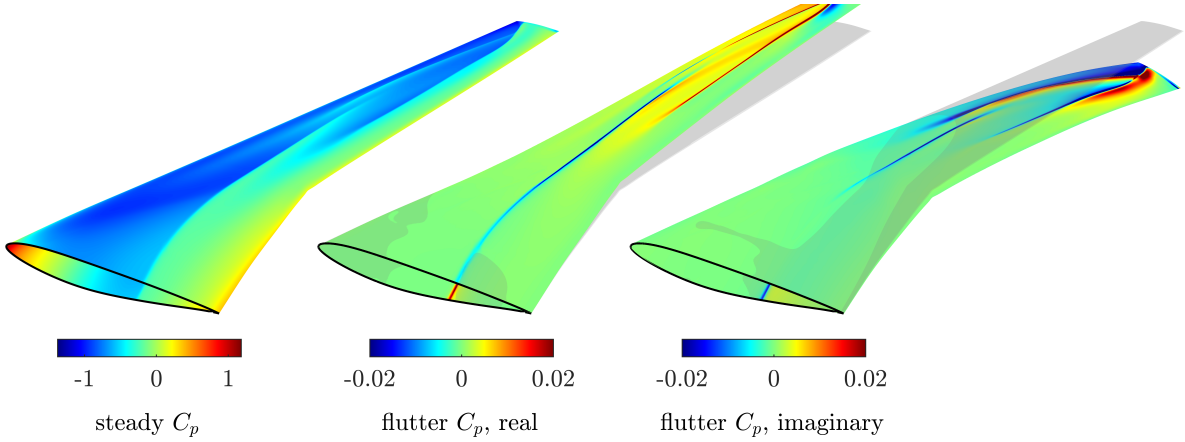

Figure 6: Surface pressure for the uCRM wing for Mach 0.85 at the flutter point.

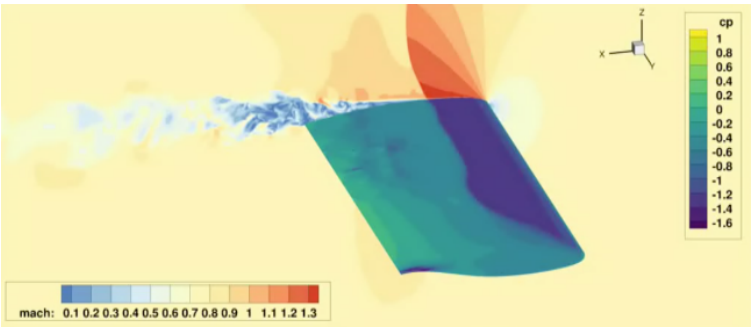

Figure 7: BSCW DDES flow field for Mach 0.8, AoA=5.0°.

thus second-order derivatives are required. A complete derivation of this process is not provided here (see Ref. 11), but some key issues are highlighted. For example, one term that must be computed is:

$$\left[\frac{\partial \boldsymbol{A}_{LFD}}{\partial \hat{\boldsymbol{q}}}\right]^T \cdot \boldsymbol{\psi} = \left(i \cdot \omega \cdot \boldsymbol{M} + \frac{\partial \boldsymbol{R}}{\partial \boldsymbol{q}}\right)^T \cdot \boldsymbol{\psi} \tag{3}$$

where $\boldsymbol{\psi}$ is an adjoint vector. This complex-valued term is a relatively straightforward matrix-vector product.

Alternatively, another term that must be computed is:

$$\frac{\partial}{\partial \boldsymbol{q}}\left(\left.\frac{\partial \boldsymbol{R}}{\partial \boldsymbol{q}}\right|_{\boldsymbol{q}_0} \cdot \hat{\boldsymbol{q}}\right) \tag{4}$$

This product has the form of a directional derivative of the first-order derivative in the direction of the vector that it is multiplying by. This term can be thought of as the derivative of $\frac{\partial \boldsymbol{R}}{\partial \boldsymbol{q}}$ with respect to $\boldsymbol{q}$ in the direction of $\hat{\boldsymbol{q}}$. Rather than computing this second-order partial derivative (and other similar terms) analytically, directional finite-difference derivatives can be used. Furthermore, because all of the first-order partial derivatives are real-valued, complex-step directional derivatives allow the linearization to be done within machine accuracy:

$$\frac{\partial}{\partial \boldsymbol{q}}\left(\left.\frac{\partial \boldsymbol{R}}{\partial \boldsymbol{q}}\right|_{\boldsymbol{q}_0} \cdot \hat{\boldsymbol{q}}\right) \approx \frac{imag\left(\left.\frac{\partial \boldsymbol{R}}{\partial \boldsymbol{q}}\right|_{\boldsymbol{q}_0 + i \cdot h \cdot real(\hat{\boldsymbol{q}})}\right)}{h} + i \cdot \frac{imag\left(\left.\frac{\partial \boldsymbol{R}}{\partial \boldsymbol{q}}\right|_{\boldsymbol{q}_0 + i \cdot h \cdot imag(\hat{\boldsymbol{q}})}\right)}{h} \tag{5}$$

where h is the complex-step size, which can be very small (10^{-30}-10^{-50}).

Additional complications arise from the fact that the flutter outputs are real-valued, but the GAF inputs to the $p-k$ solvers are complex-valued. These cost functions do not satisfy the Cauchy-Riemann equations

for complex differentiation, and therefore the adjoint equations need to be appropriately modified. Following Ref. 35, for a cost function f (i.e., flutter-q), a complex-valued state vector $\boldsymbol{y} = \boldsymbol{a} + i \cdot \boldsymbol{b}$, and a design parameter x, the total derivative is written as:

$$\begin{aligned} \frac{df}{dx} &= \frac{\partial f}{\partial x} + \frac{\partial f}{\partial \boldsymbol{a}} \cdot \frac{d\boldsymbol{a}}{dx} + \frac{\partial f}{\partial \boldsymbol{b}} \cdot \frac{d\boldsymbol{b}}{dx} \\ &= \frac{\partial f}{\partial x} + real\left[\left(\frac{\partial f}{\partial \boldsymbol{a}} - i \cdot \frac{\partial f}{\partial \boldsymbol{b}}\right) \cdot \left(\frac{d\boldsymbol{a}}{dx} + i \cdot \frac{d\boldsymbol{b}}{dx}\right)\right] \\ &= \frac{\partial f}{\partial x} + real\left[\left(\frac{\partial f}{\partial \boldsymbol{a}} - i \cdot \frac{\partial f}{\partial \boldsymbol{b}}\right) \cdot \frac{d\boldsymbol{y}}{dx}\right] \end{aligned} \tag{6}$$

For the actual LFD cases considered here, the analogy to the complex-value inputs $\boldsymbol{y}$ are the GAFs, and so the flutter derivatives with respect to the GAFs must be handled as in Eq. 6.

Flutter-q derivatives with respect to Mach number are shown in Fig. 8 for the AGARD 445.6 case, where the flutter boundary itself is also compared with results from the FUN3D/FV (finite volume) workflow. The computed sensitivities at two Mach numbers in Fig. 8 are compared to real-valued finite differences in Table 1. The adjoint and finite difference derivatives agree to five digits for $h = 10^{-5}$ at the subsonic Mach number and to six digits for $h = 10^{-7}$ at the supersonic Mach number. It is important to note that the derivatives cannot be verified to machine precision using methods such as complex-step as would normally be done, since the LFD adjoint technique used here relies on complex-step itself to compute derivatives (Eq. 5).

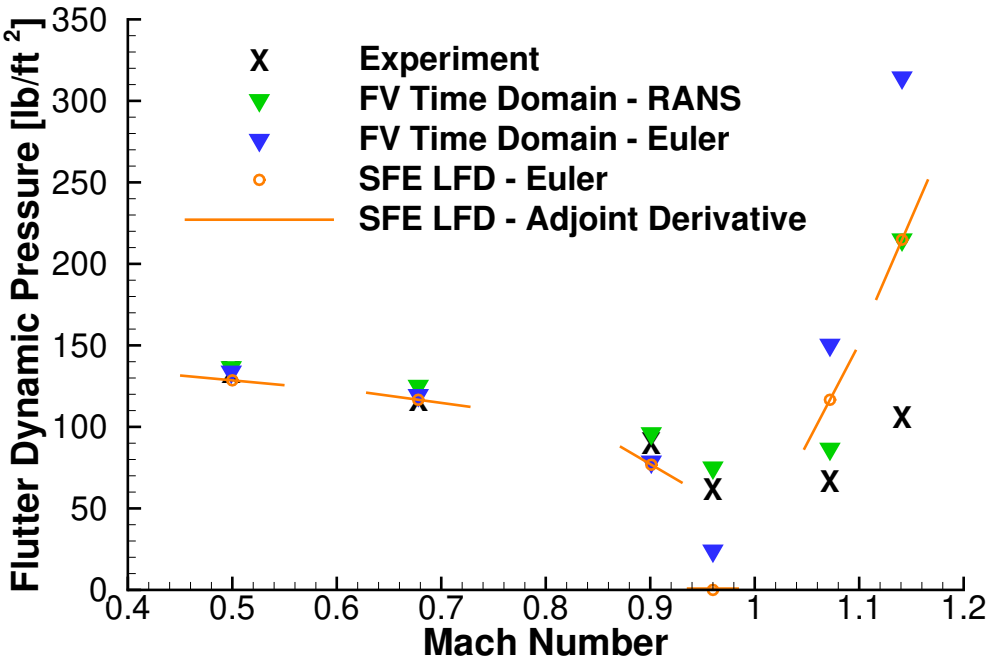

Figure 8: Flutter boundary of the AGARD 445.6 wing. FUN3D Finite volume (FV) solutions from Ref.5.

Figure 8 and Table 1 focus on flutter derivatives with respect to a flow parameter (Mach number), but derivatives with respect to shape (i.e., wing span) and sizing variables (i.e., skin thickness) are also readily available. In order to ease the barrier of entry for use of the LFD tool (and its derivatives) during design optimization, an OpenMDAO-centric[36] approach has been taken, namely via the Mphys library.[37] Mphys has been developed as a collaborative effort seeking to standardize high-fidelity multiphysics problems (in this case, unsteady aeroelastic problems) in OpenMDAO. The Mphys library also provides utilities to help set up these multiphysics optimizations that can quickly grow in complexity. A key feature of this library is swappable fidelity, provided that both fidelity analyses can match the same standardized interfaces. The LFD tool can be replaced with a lower-fidelity DLM solver without modifying other aspects of the optimization problem. Similarly, the structural model or load and displacement transfer scheme may be swapped without modifying the aerodynamic solver setup.

Table 1: Sensitivities of the flutter dynamic pressure with respect to Mach number for the AGARD 445.6 using LFD.

	$M_\infty = 0.5$	$M_\infty = 1.072$
Adjoint	−59.6929941	1225.945250
Finite Difference (10^{-4})	−59.7222326	1248.034599
Finite Difference (10^{-5})	−59.6930351	1245.346810
Finite Difference (10^{-6})	−59.6926180	1226.022198
Finite Difference (10^{-7})	−59.6874500	1225.946330
Finite Difference (10^{-8})	−59.6376992	1225.944700

A simplified view of the Mphys-generated aeroelastic workflow can be seen in the extended design structure matrix (XDSM) diagram[38] of Fig. 9, where 1) a design optimizer dictates shape and sizing design optimization variables; 2) the geometry component uses the shape variables to determine coordinates of the aerodynamic ($\boldsymbol{x_{aero}}$) and structural ($\boldsymbol{x_{struct}}$) nodes on the wing; 3) a flow solver computes the steady flow vector $\boldsymbol{q}_0$; 4) a structural modal analysis computes the matrix of structural mode shapes $\boldsymbol{\Phi}_{struct}$; 5) those mode shapes are interpolated onto the aerodynamic surface to form $\boldsymbol{\Phi}_{aero}$; 6) the LFD solver computes the GAFs $\overline{\boldsymbol{A}}$; 7) a $p-k$ method computes the flutter metric of interest. In addition to the GAFs, the inputs to the $p-k$ method are the reduced mass $\overline{\boldsymbol{M}}$, damping $\overline{\boldsymbol{C}}$, and stiffness matrices $\overline{\boldsymbol{K}}$. In order to replace LFD with linear DLM, the workflow is the same as Fig. 9, with the exception that the steady flow solution is not fed into the unsteady aerodynamic DLM (and is not in fact needed at all). The result in Fig. 9 is only valid for non-lifting flows; for lifting flows with a static aeroelastic component, a substantially more complex OpenMDAO model is required (see Ref. 39).

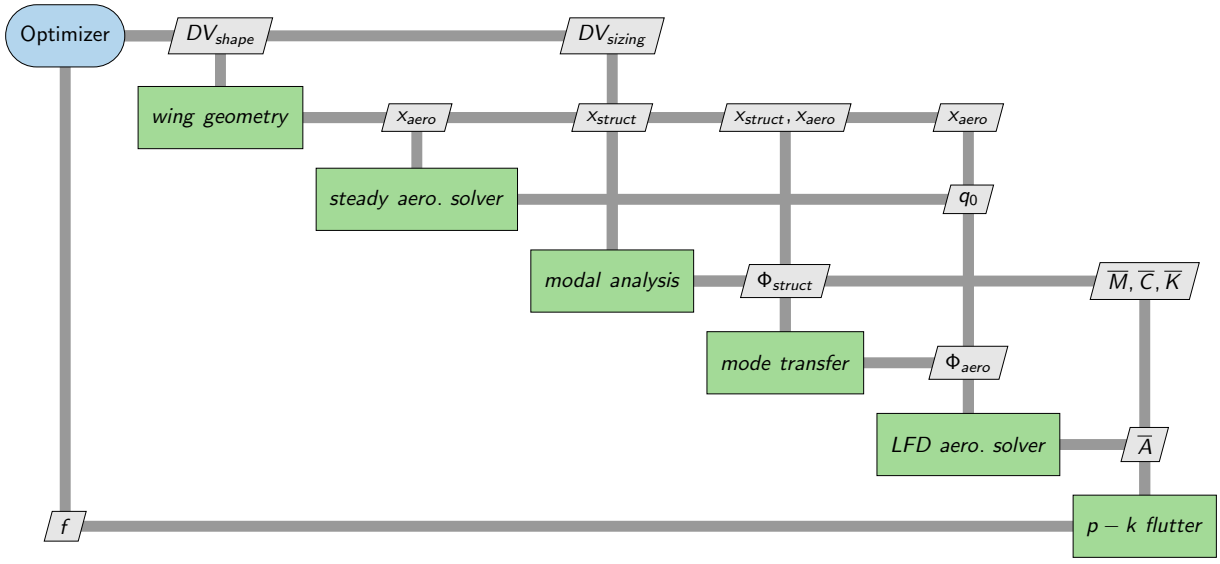

Figure 9: XDSM diagram of the aeroelastic flutter optimization process.

Sample optimization results are shown in Fig. 10 for the AGARD 445.6 case, where shape and sizing design variables are used to minimize structural mass under a flutter constraint and a planform area constraint. Specifically, an aggregated eigenvalue constraint[40] is used to push all of the eigenvalues' real part out of some "keep-out zone", effectively enforcing a flutter constraint. Four shape variables include changes to the root chord, tip chord, wing span, and wing sweep; 100 panel thicknesses are used to size the plate structure. Optimal results are shown for the DLM-based workflow and the LFD-based workflow at Mach 0.5, with minor differences between the two for this particular case. Though not demonstrated here, the Mphys library provides a means to schedule fidelity during the optimization process (i.e. complete an optimization

with the inexpensive DLM-based solver, and use this as a starting point for the LFD-based solver), or more sophisticated multi-fidelity optimization schemes.

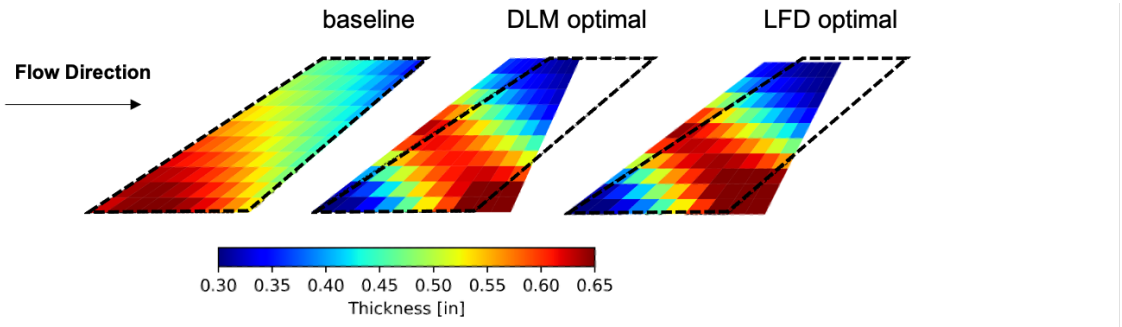

Figure 10: Shape and sizing optimization of the AGARD 445.6 wing.

In addition to design optimization, the existence of flutter derivatives can also help alleviate the computational cost of uncertainty quantification (UQ). The design and certification of flight structures requires the demonstration of a flutter margin, where the aeroelastic flutter boundary must remain outside the flight envelope by a 15% margin, as measured by equivalent air speed. This margin has been in use for decades, and is largely empirical.[41] It may be preferable to replace these empirical margins with probabilistic representations (namely, probability of flutter/failure), to help account for deviations in structural and inertial properties within a fleet[42] and also the fact that transonic flutter can be highly sensitive to uncertainties in the manufactured wing shape.[43] The cost of sampling-based UQ tools such as polynomial chaos expansion (PCE) can be reduced with derivative enrichment,[44] while other methods rely entirely on the existence of a gradient-based search to estimate reliability.[45]

An example UQ process is shown in Fig. 11, where a PCE is used to model an uncertain flutter boundary for the uCRM at both subsonic conditions (Mach 0.6) and transonic conditions (Mach 0.85). Six random variables are considered: 1) the thickness of the inboard skins; 2) the thickness of the outboard skins; 3) the thickness of the inboard spars; 4) the thickness of the outboard spars; 5) the thickness of the ribs; 6) the orientation of the skin stiffeners. For each standard normal variable, the mean value is taken from the standard uCRM layout,[16] along with a coefficient of variation (CV) of 0.05. Probability density functions (PDF) of the LFD-computed flutter-q are shown in the upper right, via a 3rd-order PCE with 168 samples: 84 samples are required to prevent an under-determined system, and Ref. 46 recommends an over-sampling factor of 2. Alternatively, a gradient-enhanced PCE can reduce the number of samples required by a factor of ten, with little discernible shift in the resulting PDFs. Global sensitivity indices[47] are shown in the upper right of Fig. 11, with the stiffener orientation variable (which will have a large impact on the bend-twist coupling of the wing) showing the largest impact on the flutter boundary.

IV. Aeroelastic Validation

The previous sections of this paper have detailed recent progress in the ability to efficiently compute transonic flutter mechanisms and the sensitivity of those mechanisms to input parameters. The final section of this work will detail ongoing and planned work for experimental model validation. As noted above, there is a lack of aeroelastic experimental datasets available for validation, with a particular interest in the validity boundary of uRANS-based methods (such as LFD). In the existing literature, the AGARD 445.6 case[4] is widely used for validation (shown here in Fig. 8 as well), but this wing is very thin and is tested at a 0.0° AoA. Ref. 5 has found that the range of Mach numbers at which nonlinear (mixed) flow exists over the wing surface is very narrow, between 0.98 and 1.01. None of the experimental data points exist in this Mach range, and so therefore: nonlinear CFD is not required to capture the experimentally-measured flutter dip, a dip which is driven entirely by compressible flow. The AGARD 445.6 test case is not a useful CFD validation test case. As summarized above, additional experimental datasets available in the literature also suffer from various flaws.

A series of tests are planned for the TDT, in an attempt to provide validation datasets for transonic aeroelastic flutter. These tests present a building block approach of progressively-complex models (rigid model, rigid model attached to a pitch-plunge apparatus, flexible model) to incrementally validate targeted

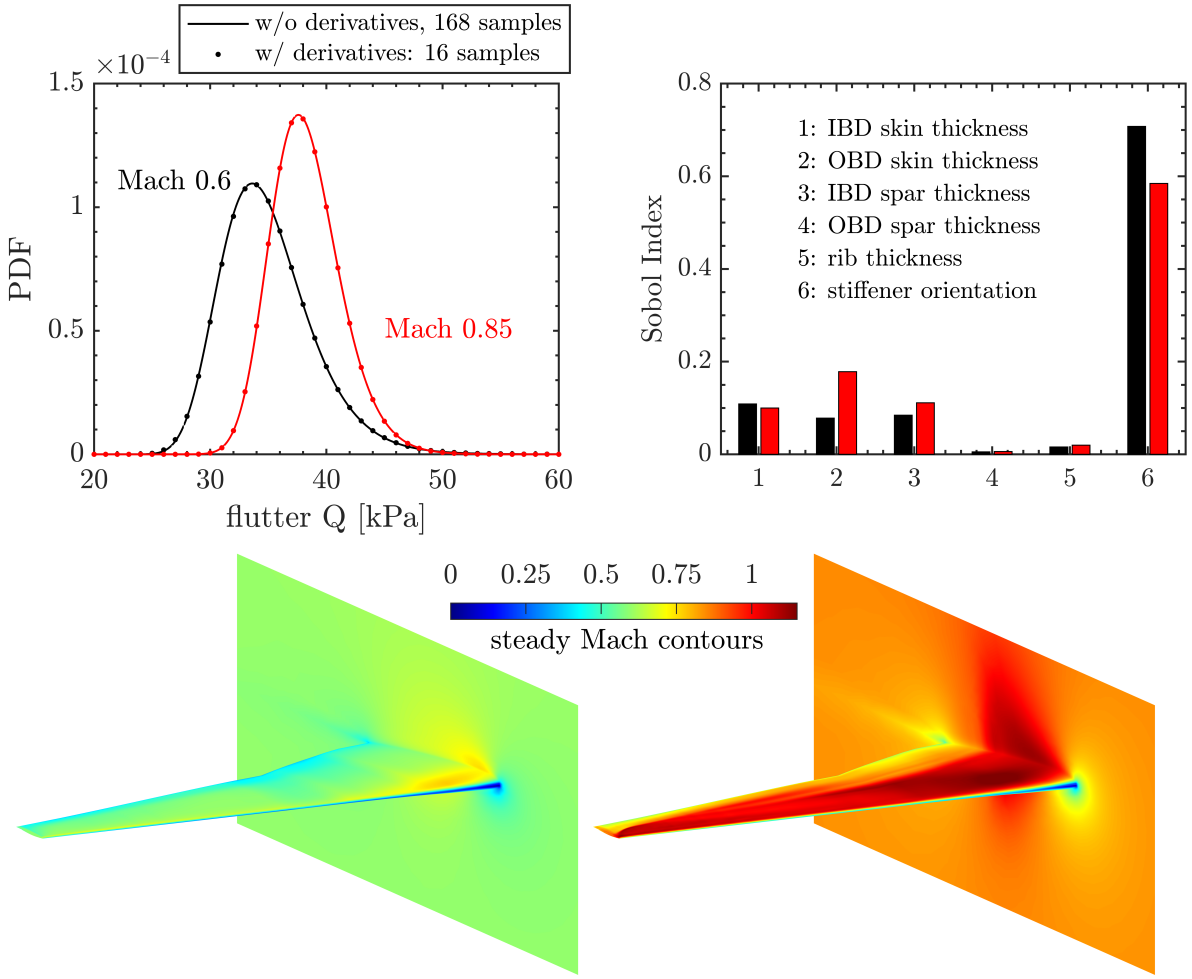

Figure 11: PCE modeling of an uncertain uCRM flutter boundary at Mach 0.6 and 0.85: probability density functions (top left); global sensitivity indices (top right); steady Mach field contours at 0.6 (bottom left) and 0.85 (bottom right).

aspects of the computational aeroelastic predictions. The first planned entry is a test of the Coe generic launch vehicle:[15] this model contains a relatively simple geometry, and a nominally rigid structure. The goals of this first test are to assess the utility of unsteady pressure sensitive paint (uPSP) and unsteady particle image velocimetry (PIV). uPSP is of particular interest: the Coe model has been tested with uPSP in Ref. 48, but the future test objectives in the TDT also include testing in the oxygen-deprived R134a medium, which is the preferred medium for flutter testing due to its higher density and lower speed of sound relative to air.

The second planned TDT entry is a retest of the BSCW, previously tested as described in Ref. 6. This model consists of a nominally rigid unswept rectangular wing (16" chord, 32" semispan) with a constant supercritical airfoil, and attached at its root to a two-degree-of-freedom pitch and lunge apparatus (PAPA). This configuration was a focus of the first two Aeroelastic Prediction Workshops,[12,13] and a planned third workshop (which also contains additional working groups focused on non-transonic aeroelasticity problems). The third workshop, and the planned re-test, has a particular focus on the data shown in Fig. 12, which is an AoA-sweep at Mach 0.8. TDT data from Ref. 6 only exists at the extremes of this plot, as the flutter-q rises to relatively high values at moderate AoA values ($2-4°$), and the resulting loads on the BSCW test apparatus became overly large. A planned re-test would attempt to fill-in the entire plot by using more detailed monitoring of the loads in the struts connecting the model to the tunnel wall, and thus more carefully approach the maximum-load limit. Failing this, the natural frequencies of the BSCW model could

be tuned to lower the flutter-q, and thus drop the peak dynamic pressure seen in Fig. 12; alternatively, the plot could be re-created at a lower Mach number, where again the peak dynamic pressure may be lower.

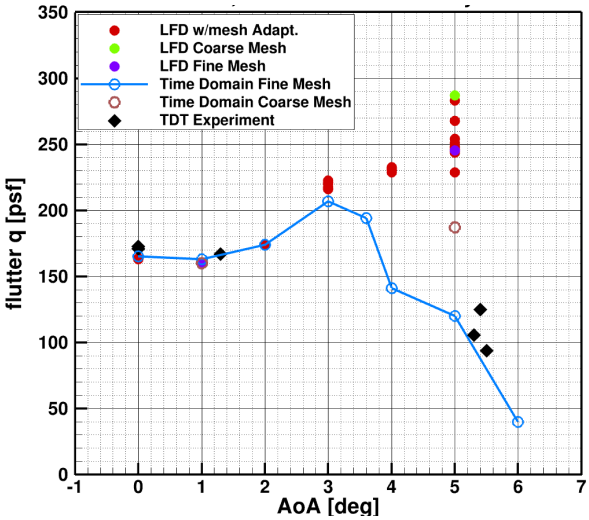

Figure 12: Flutter boundary of the BSCW at Mach 0.8.

A sweep such as seen in Fig. 12 is particularly useful for model validation, as the flows at lower AoA display a weak shock with attached flow; at the higher AoA the flow is massively separated. The static aeroelastic pressures over the wing as computed by the FUN3D/SFE solver are shown in Fig. 13, where flow separation at higher AoA is not explicitly shown, but may be inferred from the strength of the shock. For lower AoA, inviscid Euler solvers should be adequate; uRANS-based solvers will struggle at the higher AoA, and tracking the flow field across these sweeps, particularly if uPSP data is obtained across the sweep in a future test, should prove valuable for validation efforts.

It can also be seen in Fig. 12 that the LFD results (which are computed via the mesh adaptation process discussed above, and the results from the final 10 meshes are shown in the figure) shows substantially-higher flutter boundaries near 5° AoA, compared to the TDT data. It's not surprising that the LFD would be incorrect at this condition, given the massive flow separation. However, the time-domain uRANS results (which is computed on a fixed manually-constructed mesh) are in relatively good agreement at this high angle. There is some indication, however,[49] that the time-domain flutter response is very sensitive to the initial modal perturbation, with large perturbations providing relatively low flutter-q values in-line with the TDT results, and smaller values leading to higher flutter boundaries. Time domain results should approach LFD in the limit of very-small perturbations.

An additional complication with the BSCW model is the fact that it is attached to a large splitter plate at its root, offset from the tunnel wall by 40". This plate is intended to remove the BSCW from the tunnel wall boundary layer, but the plate itself has a critical Mach number of 0.8, above which a shock forms at its leading edge.[50] Given this, meaningful validation tests cannot be obtained at conditions above Mach 0.8, unless the computational model itself includes the splitter plate and (perhaps) the tunnel walls as well. An example of this can be seen in Fig. 14, where the back view shows the struts connecting the splitter plate to the tunnel wall, and a large fairing structure meant to protect the PAPA structure from the flow. The mesh and computational requirements needed to model the tunnel and the splitter plate are obviously large, and likely not suitable as a widely-used validation case. Future work will consider re-designing the shape of the splitter plate's leading edge (suggested in Ref. 50) in order to increase the critical Mach number, and allow for a greater range of wing-alone modeling.

Finally, the third planned TDT entry is an aeroelastic Common Research Model (CRM):[16] where the BSCW is a relatively simple geometry with a nominally-rigid structure (flexibility derived from the root PAPA mechanism), a CRM model would possess more realistic structural and geometric characteristics. The envisioned requirements for such a model are listed below.

1. A prescribed dynamic pressure flutter boundary as a function of Mach number throughout the TDT envelope, with a well-defined transonic flutter "dip," in addition to a prescribed flutter reduced frequency.

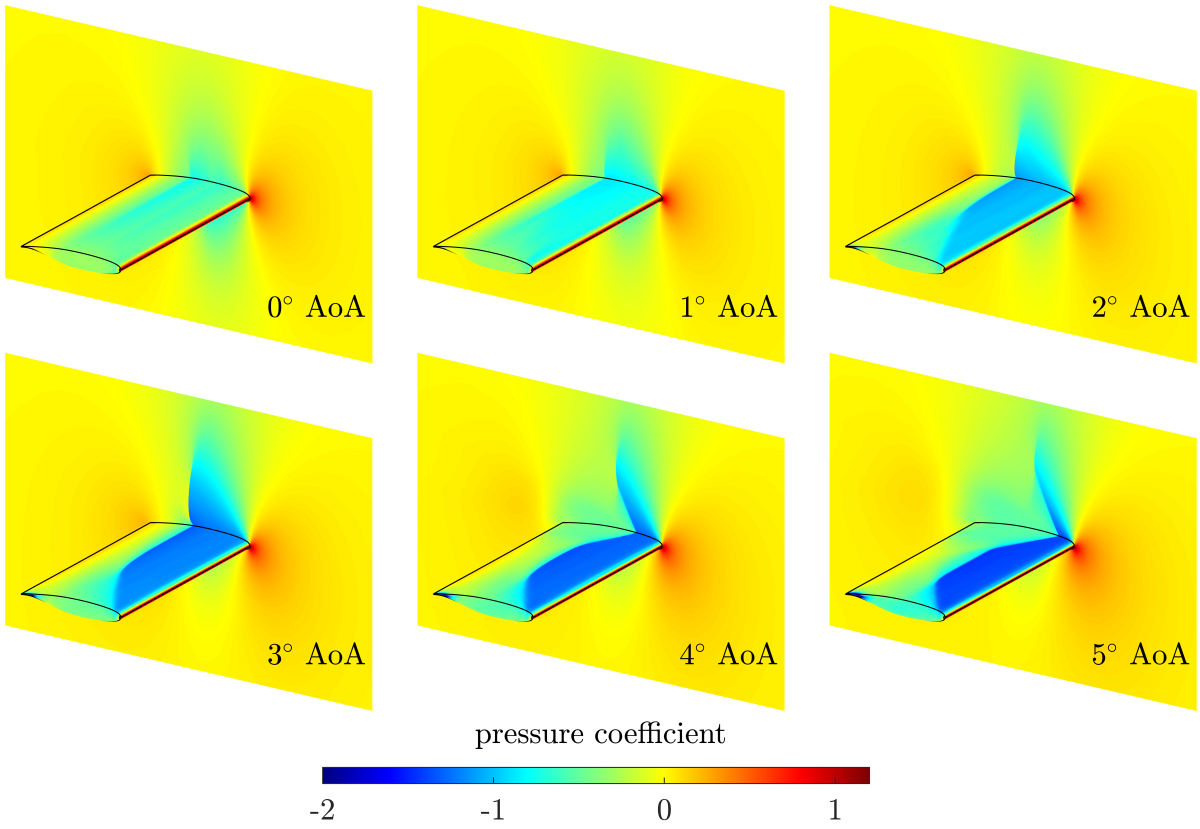

Figure 13: Steady surface pressure coefficients of the BSCW at Mach 0.8, as computed by FUN3D/SFE.

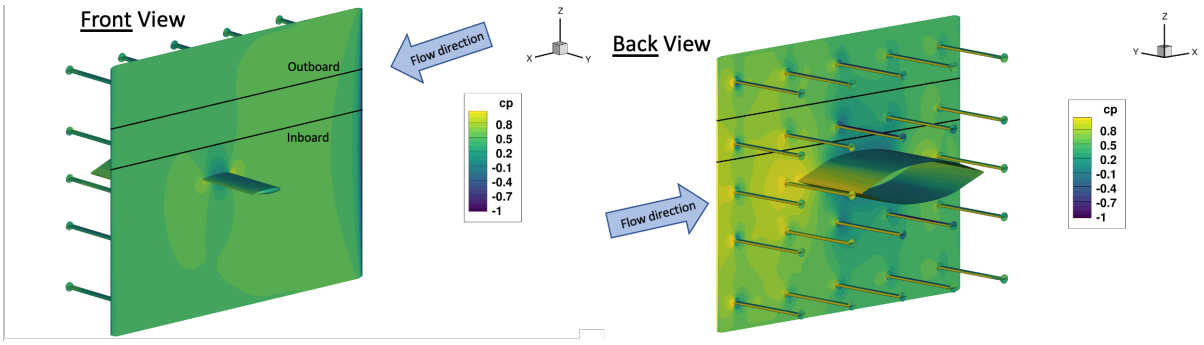

Figure 14: Snapshot of pressure coefficients over the BSCW and splitter plate: tunnel walls modeled but not shown.

2. A static aeroelastic response within required safety factors, throughout the expected operating region of the tunnel envelope.
3. A single-bodied, monolithic, well-defined outer mold line (OML) with high-quality surface finish.

The final OML requirement is driven by the fact that a consistent hallmark of aeroelastic model design is the use of stores, bodies, pylons, or wing breaks, to lower the torsional frequency of the model and allow for the occurrence of flutter at reasonably low dynamic pressures within the tunnel envelope: see Ref. 51, for example. The resulting geometry of this segmented wing-body assembly would complicate the numerical benchmarking process and is to be avoided. If flutter is to occur at a reasonably-low dynamic pressure without these conventional model design methods, then this places the onus on a highly-tuned stiffness and mass distribution inside the OML, in order to obtain the three conflicting requirements listed above. Formal

numerical aeroelastic optimization can be used to obtain a design with prescribed flutter dynamic pressures, flutter frequencies, flutter mechanisms, and static aeroelastic response.

Considering a full-span, sting-mounted model with a 10' span (scale factor of 0.052 relative to a conceptual full-scale CRM), a sample wing concept is shown in Fig. 15. A variable-thickness fiberglass plate spans the camber line of the CRM wing, with high-density foam used to maintain the jig shape OML where needed. Discrete lumps of high-density tungsten can also be utilized, and are indicated in the figure with magenta lines. The structure is optimized such that the flutter-q is 150 psf (at Mach 0.8), and a safety factor on the static stresses is at least 3, at Mach 0.8, 3° AoA, 300 psf q. This design space is marked by a strong conflict between low-stiffness (such that the model flutters where desired) and high-strength (to ensure a safe structural response). As noted, the use of tungsten helps the optimizer ease this conflict, since the large outboard inertia can help lower the flutter-q without decreasing stiffness.

The reduced flutter frequency of this model is relatively low (k=0.08), and as such, the flutter mechanism for this case is quasi-steady. In order to provide validation data which highlights fully-unsteady computations, a second model (seen in Fig. 16) is optimized to force the flutter reduced frequency to a higher value (k=0.3). The flutter boundary and static strength requirements are the same as before. The structural characteristics of Fig. 16 are substantially different than seen in Fig. 15, with a large spar-like structure nearly rigidizing the inboard portion of the wing, in order to meet the high frequency requirements. The flutter behavior for these two designs is shown in Fig. 17; where the two designs have the same flutter-q, but the low-frequency design is a coupling of modes 1 and 2, as opposed to Fig. 16 which couples modes 2 and 3.

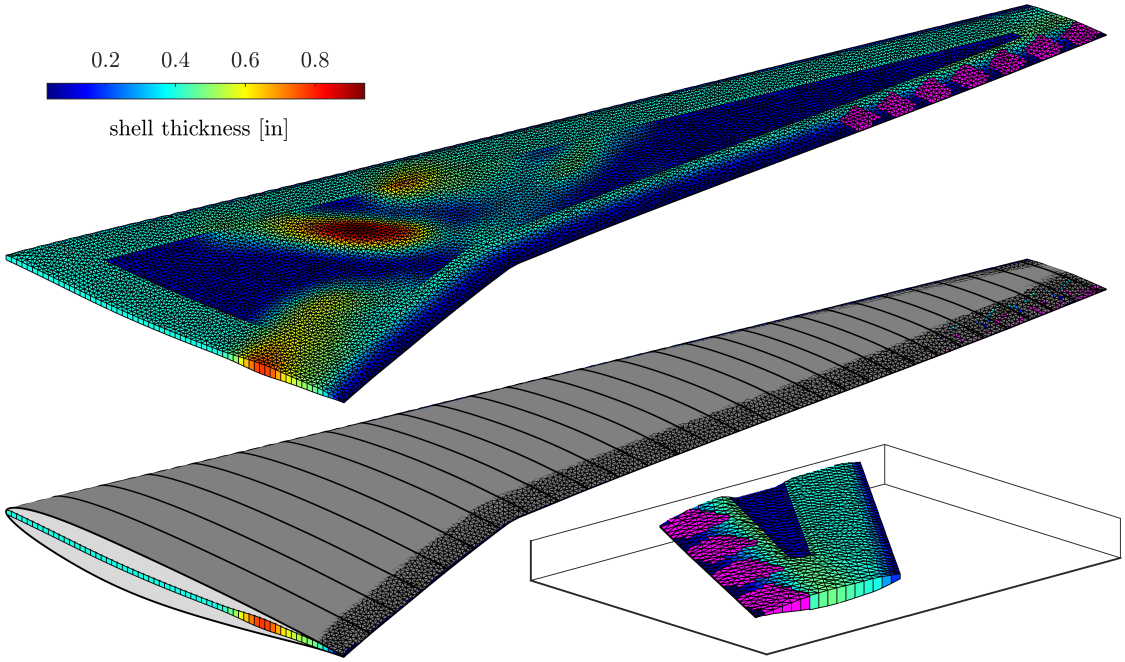

Figure 15: CRM wing structure (top) and foam OML (bottom); low flutter frequency design (k=0.08).

These designs have been optimized with lower-fidelity DLM aerodynamic predictions, as opposed to the LFD-based optimization workflow detailed above. Future work will entail CFD-based post-processing of these designs to map out the complete flutter behavior, especially the transonic flutter dips. If these designs do not display the desired transonic behavior (i.e., a strong deviation from linear predictions at higher Mach numbers, followed by a substantial post-dip rise in flutter-q), then it will be necessary to re-design these CRM models with the LFD solver, and add optimization constraints which specifically shape the q-vs-Mach curve to the desired characteristics.

V. Conclusions

This paper has provided an overview of current and planned activities at NASA Langley's Aeroelasticity Branch in the area of transonic aeroelastic prediction, design, and validation. The current state of the art

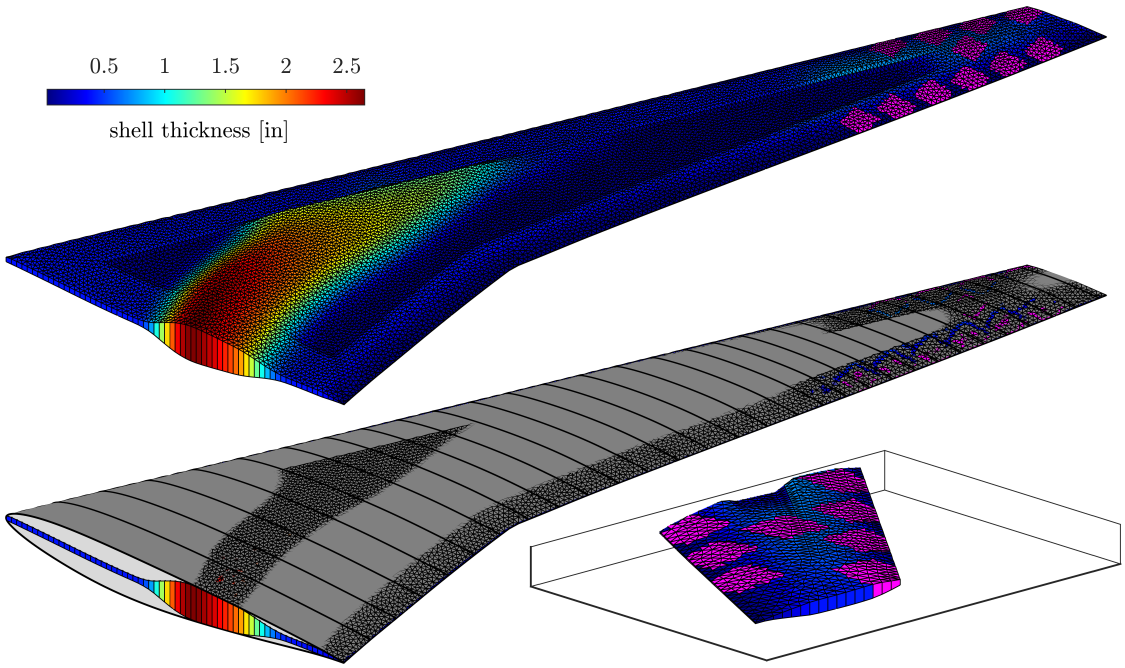

Figure 16: CRM wing structure (top) and foam OML (bottom); high flutter frequency design (k=0.30).

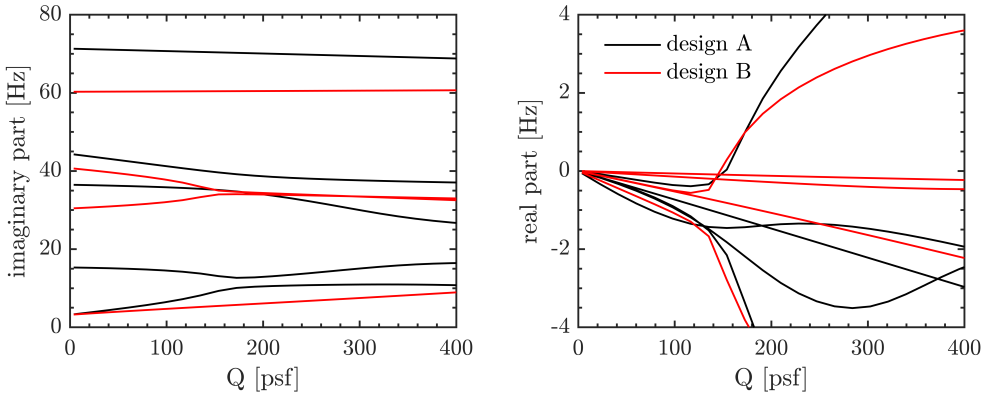

Figure 17: Flutter behavior for the design of Fig. 15 (A) and Fig. 16 (B).

in computational aeroelasticity struggles to accurately predict flutter dip behavior in transonic flow, given that this dip geometry is strongly influenced by nonlinearities in the flow. An inability to predict this behavior has important ramifications for design, as a flutter boundary may drop into a flight envelope at off-design conditions. Techniques used for past aircraft design avoid a direct accounting of transonic flutter (due to its high cost), and instead rely on lower fidelity predictions and an added degree of conservatism. Nontraditional vehicle concepts under consideration for future development, however, may be more flutter-critical than current aircraft (e.g., large wing spans for drag-reduction purposes); for these vehicles, it may not be possible to properly design the vehicle using flutter predictions from lower-fidelity aeroelastic analysis tools.

CFD-based aeroelastic predictions can be made more tractable with the linearized frequency-domain (LFD) method, which provides direct flutter boundaries without a costly and cumbersome time-domain analysis. The outputs from a LFD solver (i.e., generalized aerodynamic forces) are identical in form to those found from conventional linear tools. The adjoint-based flutter derivatives from the LFD process are also tractable, and can then be used for large-scale high-fidelity design optimization with flutter constraints,

uncertainty quantification, etc. Beyond challenges with numerical prediction and design, there is also a lack of existing experimental datasets for use in validation. Specifically, the limits of uRANS solvers are not well-understood for predicting flows with strong nonlinearities, and when higher-fidelity tools (i.e., DDES, LES) are needed for flutter computations. To address this gap, future testing plans have been presented here for a series of progressively-complex wind tunnel tests.

Acknowledgments

This work is supported by the Transformational Tools and Technologies (TTT) project of the NASA Transformative Aeronautics Concepts Program (TACP). Computational resources for this work are provided by the NASA Langley K cluster.

References

[1]Gates, D., "In Person: Fitzgerald's Fix for the Boeing 747-8 Earns Aviation Honors," *Seattle Times*, http://www.seattletimes.com/business/in-person-fitzgeralds-fix-for-boeing-747-8-earns-aviation-honors [retrieved 2021].

[2]Cooper, J., "Towards Faster and Safer Flight Flutter Testing," RTO AVT Symposium on Reduction of Military Vehicle Acquisition Time and Cost Through Advanced Modeling and Virtual Simulation, NATO Paper 089, March 2003.

[3]Edwards, J., "Calculated Viscous and Scale Effects on Transonic Aeroelasticity," *Journal of Aircraft*, Vol. 45, No. 6, pp. 1863-1871, 2008.

[4]Yates, C., "AGARD Standard Aeroelastic Configurations for Dynamic Response. Candidate Configuration I - Wing 445.6," NASA TM-100492, August,1987.

[5]Silva, W., Chwalowski, P., Boyd, P., "Evaluation of Linear, Inviscid, Viscous, and Reduced-Order Modeling Aeroelastic Solutions of the AGARD 445.6 Wing using Root Locus Analysis" *International Journal of Computational Fluid Dynamics*, Vol. 28, No. 3, pp. 122-139, 2014.

[6]Bennett, R., "Test Cases for Flutter of the Benchmark Models Rectangular Wings on the Pitch and Plunge Apparatus," Defense Technical Information Center TR ADPO10713, Fort Belvoir, VA, 2000.

[7]Zwaan, R., "Verification of Calculation Methods for Unsteady Airloads in the Prediction of Transonic Flutter" *Journal of Aircraft*, Vol. 22, No. 10, pp. 833-839, 1985.

[8]Edwards, J., Spain, C., Keller, D., Moses, R., Schuster, D., "Transport Wing Flutter Model Transonic Limit Cycle Oscillation Test," *Journal of Aircraft*, Vol. 46, No. 4, pp. 1104-1113, 2009.

[9]Moeljo, H., Bhatia, K., SenGupta, G., Kim, T., Kuruvila, G., Silva, W., Bartels, R., Biedron, R., "Simulations of a Twin-Engine Transport Flutter Model in the Transonic Dynamics Tunnel," IFASD paper 2003-US-44.

[10]Jacobson, K., Stanford, B., Wood, S., Anderson, W., "Frequency-Domain Flutter Analysis and Sensitivities with Stabilized Finite Elements," *AIAA SciTech Forum*, Orlando, FL, January 6-10, 2020.

[11]Jacobson, K., Stanford, B., Wood, S., Anderson, W., "Adjoint-based Sensitivities of Flutter Predictions based on the Linearized Frequency-Domain Approach," *AIAA SciTech Forum*, January 2021.

[12]Heeg, J., Chwalowski, P., Florance, J., Wieseman, C., Schuster, D., Perry, B., "Overview of the Aeroelastic Prediction Workshop," *AIAA Aerospace Sciences Meeting*, Grapevine, TX, January 7-10, 2013.

[13]Heeg, J., Wieseman, C., Chwalowski, P., "Data Comparisons and Summary of the Second Aeroelastic Prediction Workshop," *AIAA Aviation Forum*, Washington DC, June 13-17, 2016.

[14]Oberkampf, W., Smith, B., "Assessment Criteria for Computational Fluid Dynamics Model Validation Experiments," *Journal of Verification, Validation, and Uncertainty Quantification*, Vol. 2, No. 3, 2017.

[15]Coe, C., Nute, J., "Steady and Fluctuating Pressures at Transonic Speeds on Hammerhead Launch Vehicles," NASA TM X-778, 1962.

[16]Brooks, T., Kenway, G., Martins, J., "Benchmark Aerostructural Models for the Study of Transonic Aircraft Wings," *AIAA Journal*, Vol. 56, No. 7, pp. 2840-2855, 2018.

[17]Bartels, R., Rumsey, C., Biedron, R., "CFL3D Version 6.4 - General Usage and Aeroelastic Analysis," NASA TM 2006-214301.

[18]Jacobson, K., Kiviaho, J., Kennedy, G., Smith, M., "Evaluation of Time-Domain Damping Identification Methods for Flutter-Constrained Optimization," *Journal of Fluids and Structures*, Vol. 87, pp. 174-188, 2019.

[19]Stanford, B., Massey, S., "Uncertainty Quantification of the FUN3D-Predicted NASA CRM Flutter Boundary," *AIAA SciTech Forum*, Grapevine, TX, January 9-13, 2017.

[20]Thormann, R., Widhalm, M., "Linear-Frequency-Domain Predictions of Dynamic-Response Data for Viscous Transonic Flows," *AIAA Journal*, Vol. 51, No. 11, pp. 2540-2557, 2013.

[21]Bekemeyer, P., Thormann, R., Timme, S., "Frequency-Domain Gust Response using Computational Fluid Dynamics," *AIAA Journal*, Vol. 55, No. 7, pp. 2154-2187, 2017.

[22]Anderson, W., Newman, J., Karman, S., "Stabilized Finite Elements in FUN3D," *Journal of Aircraft*, Vol. 55, No. 2, pp. 696-714, 2017.

[23]Biedron, R., Carlson, J., Derlaga, J., Gnoffo, P., Hammond, D., Jacobson, K., Jones, W., Kleb, B., Lee-Rausch, E., Nielsen, E., Park, M., Rumsey, C., Thomas, J., Thompson, K., Walden, A., Wang, L., Wood, W., "FUN3D Manual: 13.7," NASA TM-2020-5010139.

[24]Stanford, B., Jacobson, K., "Transonic Aeroelastic Modeling of the NACA 0012 Benchmark Wing," *AIAA Journal*, Vol. 59, No. 10, pp. 4134-4143, 2021.

[25]Jacobson, K., Stanford, B., Kiviaho, J., Ozoroski, T., Park, M., Chwalowski, P., "Multiscale Mesh Adaptation for Transonic Aeroelastic Flutter Problems," *AIAA Aviation Forum*, virtual event, 2021.

[26]Waite, J., Bartels, B., Stanford, B., "Aeroelastic Model Development for the Integrated Adaptive Wing Technology Maturation Project Wind Tunnel Test," *AIAA Aviation Forum*, virtual event, 2020.

[27]Massey, S., Stanford, B., Jacobson, K., "FUN3D Aeroelastic Analysis of the X-56A for the Third Aeroelastic Prediction Workshop" *AIAA Scitech Forum*, 2022, to appear.

[28]Vatsa, V., Lockard, D., Spalart, P., "Grid Sensitivity of SA-Based Delayed-Detached-Eddy-Simulation Models for Blunt-Body Flows," *AIAA Journal*, Vol. 55, No. 8, pp. 2842–2847, 2017.

[29]Mani, K., Mavriplis, D., "Adjoint-Based Sensitivity Formulation for Fully Coupled Unsteady Aeroelasticity Problems," *AIAA Journal*, Vol. 47, No. 8, pp. 1902–1915, 2009.

[30]Walden, A., Nielsen, E., Diskin, B., Zubair, M., "A Mixed Precision Multicolor Point-Implicit Solver for Unstructured Grids on GPUs," *IEEE/ACM 9th Workshop on Irregular Applications: Architectures and Algorithms*, Denver, CO, November 18, 2019.

[31]Kessler, D., Hess, A., Obenshain, K., Eder, D., Koniges, A., Candler, G., Johnson, H., Bretheim, J., Roe, K., McDaniel, D., Bond, R., Nielsen, E., Walden, A., Nastac, G., Jacobson, K., Campbell, R., "Performance of Coupled Physics Solvers for Multidisciplinary Hypersonic Flow Simulations on Several Classes of Computer Architectures," *AIAA SciTech Forum*, 2022, to appear.

[32]Zhang, Z., Chen, P., Yang, S., Wang, Z., Wang, Q., "CFD-Based Aeroelastic Adjoint Sensitivities for Flight Vehicle Weight Minimization using Sizing and Shape Design Variables," *AIAA SciTech Forum*, Grapevine, TX, January 9-13, 2017.

[33]Jacobson, K., Kiviaho, J., Kennedy, G., Smith, M.,"An Aeroelastic Coupling Framework for Time-Accurate Analysis and Optimization," *AIAA SciTech Forum*, Kissimmee, FL, January 8-12, 2018.

[34]Wang, Q., Moin, P., Iaccarino, G., "Minimal Repetition Dynamic Checkpointing Algorithm for Unsteady Adjoint Calculation," *SIAM Journal of Scientific Computing*, Vol. 31, No. 4, pp. 2549–2567, 2009.

[35]Igarashi, H., Watanabe, K., "Complex Adjoint Variable Method for Finite-Element Analysis of Eddy Current Problems," *IEEE Transactions on Magnetics*, Vol. 46, No. 8, pp. 2739–2742, 2010.

[36]Gray, J., Hwang, J., Martins, J., Moore, K., Naylor, B., "OpenMDAO: An Open-Source Framework for Multidisciplinary Design, Analysis, and Optimization," *Structural and Multidisciplinary Optimization*, Vol. 59, No. 4, pp. 1075-1104, 2019.

[37]Yildirim, A., Jacobson, K., Stanford, B., Gray, J., Mader, C., Martins, J., Kennedy, G., "A Modular Multiphysics Simulation Framework Using OpenMDAO," *AIAA Aviation Forum*, virtual event, June 15-19, 2020.

[38]Lambe, A., Martins, J., "Extensions to the Design Structure Matrix for the Description of Multidisciplinary Design, Analysis, and Optimization Processes" *Structural and Multidisciplinary Optimization*, Vol. 46, pp. 273-284, 2012.

[39]Jacobson, K., Stanford, B., "Flutter-Constrained Optimization with the Linearized Frequency-Domain Approach" *AIAA Scitech Forum*, 2022, to appear.

[40]Stanford, B., "Role of Unsteady Aerodynamics During Aeroelastic Optimization" *AIAA Journal*, Vol. 53, No. 12, pp. 3826–3831, 2015.

[41]Pettit, C., "Uncertainty Quantification in Aeroelasticity: Recent Results and Research Challenges," *Journal of Aircraft*, Vol. 41, No. 5, pp. 1217-1229, 2004.

[42]Pitt, D., Haudrich, D., Thomas, M., Griffin, K., "Probabilistic Aeroelastic Analysis and Its Implications on Flutter Margin Requirements," *AIAA Structures, Structural Dynamics, and Materials Conference*, Schaumburg, IL, April 2008.

[43]Housman, J., Kiris, C., "Overset Grid Simulations for the Second AIAA Aeroelastic Prediction Workshop," *AIAA SciTech Forum*, Grapevine, TX, January 2017.

[44]Roderick, O., Anitescu, M., Fischer, P., "Polynomial Regression Approaches Using Derivative Information for Uncertainty Quantification," *Nuclear Science and Engineering*, Vol. 164, pp. 122-139, 2010.

[45]Rackwitz, R., "Reliability Analysis - A Review and Some Perspectives," *Structural Safety*, Vol. 23, No. 4, pp. 365-395, 2001.

[46]Hosder, S., Walters, R., Balch, M., "Point-Collocation Nonintrusive Polynomial Chaos Method for Stochastic Computational Fluid Dynamics," *AIAA Journal*, Vol. 48, No. 12, pp. 2721-2730, 2010.

[47]Sudret, B., "Global Sensitivity Analysis Using Polynomial Chaos Expansion," *Reliability Engineering and System Safety*, Vol. 93, No. 7, 2008, pp. 964-979.

[48]Schuster, D., Panda, J., Ross, J., Roozeboom, N., Burnside, N., Ngo, C., Kumagai, H., Sellers, M., Powell, J., Sekula, M., Piatak, D., "Investigation of Unsteady Pressure-Sensitive Paint (uPSP) and Dynamics Loads Balance to Predict Launch Vehicle Buffet Environments," NASA TM-2016-219352.

[49]Chwalowski, P., Massey, S., Jacobson, K., Silva, W., Stanford, B., "Progress on Transonic Flutter and Shock Buffet Computations in Support of the Third Aeroelastic Prediction Workshop" *AIAA Scitech Forum*, 2022, to appear.

[50]Schuster, D., "Aerodynamic Measurements on a Large Splitter Plate for the NASA Langley Transonic Dynamics Tunnel," NASA TM-2001-210828.

[51]Stenfelt, G., Ringertz, U., "Design and Construction of Aeroelastic Wind Tunnel Models," *The Aeronautical Journal*, Vol. 119, No. 1222, pp. 1585-1599, 2015.